Mechanisms and feasibility of prey capture in ambush-feeding zooplankton

Thomas Kiørboe[a,1], Anders Andersen[b], Vincent J. Langlois[b,2], Hans Henrik Jakobsen[a], and Tomas Bohr[b]

[a]National Institute for Aquatic Resources, Technical University of Denmark, Kavalergården 6, DK-2920 Charlottenlund, Denmark; and [b]Department of Physics and Center for Fluid Dynamics, Technical University of Denmark, DK-2800 Kgs. Lyngby, Denmark

Edited by David M. Karl, University of Hawaii, Honolulu, HI, and approved June 15, 2009 (received for review March 27, 2009)

Many marine zooplankters, particularly among copepods, are "ambush feeders" that passively wait for their prey and capture them by fast surprise attacks. This strategy must be very demanding in terms of muscle power and sensing capabilities, but the detailed mechanisms of the attacks are unknown. Using high-speed video we describe how copepods perform spectacular attacks by precision maneuvering during a rapid jump. We show that the flow created by the attacking copepod is so small that the prey is not pushed away, and that the attacks are feasible because of their high velocity (≈100 mm·s^{-1}) and short duration (few ms), which leaves the prey no time for escape. Simulations and analytical estimates show that the viscous boundary layer that develops around the attacking copepod is thin at the time of prey capture and that the flow around the prey is small and remains potential flow. Although ambush feeding is highly successful as a feeding strategy in the plankton, we argue that power requirements for acceleration and the hydrodynamic constraints restrict the strategy to larger (> 0.25 mm), muscular forms with well-developed prey perception capabilities. The smallest of the examined species is close to this size limit and, in contrast to the larger species, uses its largest possible jump velocity for such attacks. The special requirements to ambush feeders with such attacks may explain why this strategy has evolved to perfection only a few times among planktonic suspension feeders (few copepod families and chaetognaths).

biological fluid dynamics | boundary layer | copepod | potential flow

Marine suspension-feeding zooplankton must concentrate dilute microplankton prey from a viscous environment, and they typically need to clear huge volumes of water (10^5 times their own volume every hour) to cover their needs (1). Two main food collection strategies have evolved: active cruising or generation of a feeding current by the beating of feeding appendages, cilia, or flagellae, and capture of prey that arrive in this current (2–4) or passive ambush feeding, where passing prey are detected and captured in surprise attacks (5–7) or as they collide with feeding structures (8). The former strategy occurs among all zooplankton taxa and size classes, from few μm-sized heterotrophic nanoflagellates to centimeter-sized krill and larger gelatinous forms (2–4). In contrast, ambush feeding with active prey attack is restricted to larger individuals and a few taxonomic groups, mainly chaetognaths and among copepods (mostly cyclopoidea), both of which are highly successful in terms of both omnipresence and high abundances (6, 9).

There are many potential advantages of ambush feeding over active prey encounter strategies. Ambush-feeding zooplankters have reduced encounters with predators, and they do not need to spend energy for swimming. These are the likely explanations that obligatory ambush-feeding copepods such as *Oithona* spp. have an order of magnitude lower metabolic rates (10, 11) and experience much lower mortalities in the ocean than similarly sized, co-occurring copepods that have more active feeding strategies (12). These are substantial fitness advantages. Why, then, is ambush feeding with active prey capture essentially restricted to a few taxonomic groups?

The hydrodynamics of the diverse mechanisms of prey capture in both protistan and metazoan feeding-current feeders have long been rather well resolved (2, 13). In copepods, for example, detection and capture of prey entrained in the feeding current has been described by using high-speed cinematography of tethered individuals: Prey are perceived remotely by using chemical signals, and the feeding current is redirected such that the detected prey comes within reach of the second maxillae (one of the feeding appendages) that captures the prey (13, 14). It is well documented that ambush-feeding copepods sense their prey remotely by using the hydrodynamic disturbances generated by the swimming prey and that the forward attack jump is faster than what can be resolved by 25- to 30-Hz video (7, 15, 16). However, it is unclear how the copepod avoids pushing the prey away as it attacks and avoids warning the prey by the hydrodynamic disturbance that the forward lunge creates. Many motile protists have the capability to sense and escape fluid deformation signals (17). However, capture efficiencies must be high, because observed clearance rates in, e.g., ambush feeding *Oithona* spp. (18, 19) accord well with those predicted from encounter models and known perception capabilities (20).

In this study we report direct high-speed video observations of prey attack and capture in small (<1 mm) free-swimming, ambush-feeding copepods. We show that attacks are successful and feasible because of their rapidity and precision and argue that hydrodynamics and power requirements limit the strategy to copepods and a few other groups in the plankton with muscular capabilities that are not found in any other invertebrates.

Results

We recorded prey attacks and escape jumps in two species, 0.8-mm *Acartia tonsa* and 0.3-mm *Oithona davisae*, with high-speed video. *O. davisae* is a mandatory ambush feeder (19), whereas *A. tonsa* can switch between the two feeding strategies (5). Although details differed, the sequence of events was very similar for the two species (see Movies S1 and S2). Prey attacks are elicited when a swimming prey comes within ≈0.2 mm of the first antenna (Fig. 1 and Table 1). In the typical attack, the copepod jumps toward the prey by sequentially striking the three or four posterior swimming legs backwards (ignoring the rudimentary fifth swimming legs in *A. tonsa*). This action pushes the copepod forward, by up to one body length and to a peak velocity of ≈100 mm·s^{-1} within a few milliseconds (Fig. 2 and Table 1), and positions it such that it has the prey about ¼ body length ventral to the feeding appendages (Fig. 1). This position is independent of the position of and distance to the prey at

Author contributions: T.K., A.A., V.J.L., H.H.J., and T.B. performed research and wrote the paper.

The authors declare no conflict of interest.

This article is a PNAS Direct Submission.

[1]To whom correspondence should be addressed. E-mail: tk@aqua.dtu.dk.

[2]Present address: Laboratoire de Sciences de la Terre, Université Claude Bernard Lyon 1, 69622 Villeurbanne Cedex, France.

This article contains supporting information online at www.pnas.org/cgi/content/full/0903350106/DCSupplemental.

www.pnas.org/cgi/doi/10.1073/pnas.0903350106

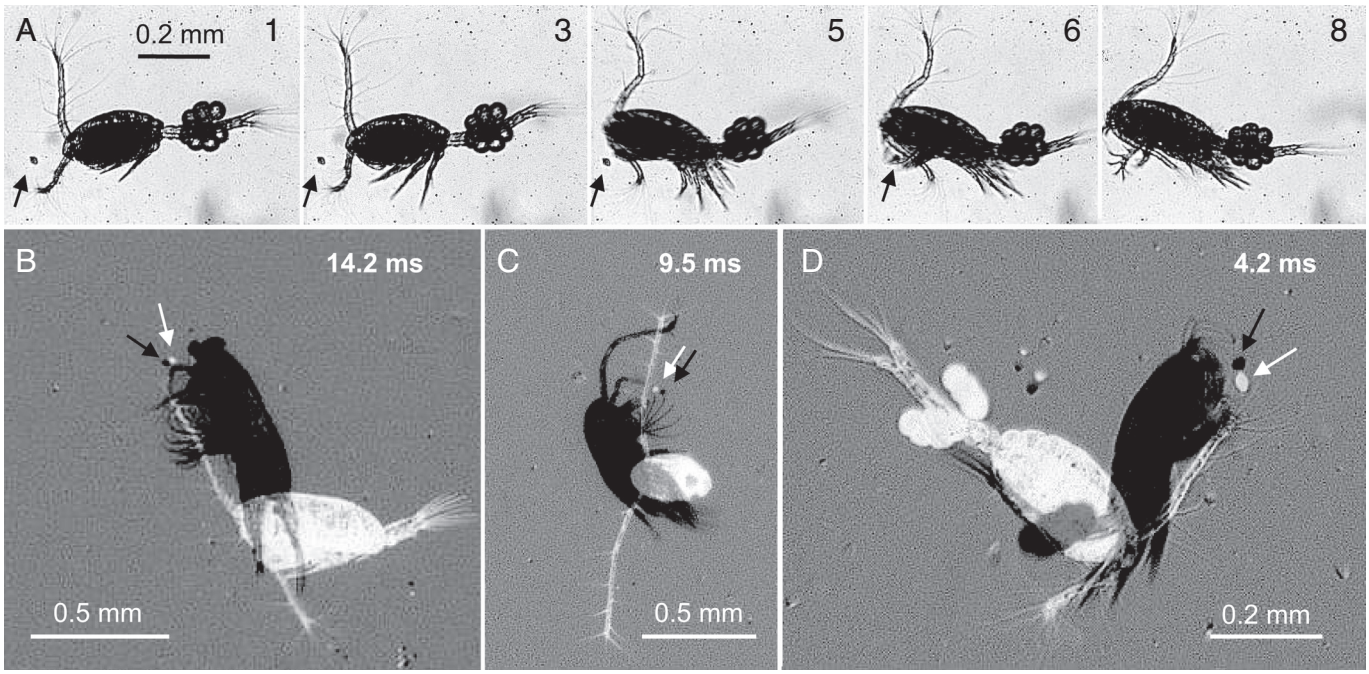

Fig. 1. Prey capture in *A. tonsa* (*B* and *C*) and *O. davisae* (*A* and *D*). Time series of still images (*A*) with frame numbers indicated (consecutive frames are 0.5 ms apart), and positions of copepod and prey immediately before (in white) and after (in black) the forward jump (*B–D*). The duration of the jumps are indicated. Note how the copepod may reorient during the attack, and how the prey hardly moves.

detection. To achieve this, the copepod steers by means of the urosome (the ''tail'') and the first antennae during the forward lunge and may demonstrate a fantastic maneuverability. In one instance, *A. tonsa* turned its body-axis 180° and further rotated 90° around its body-axis during the strike.

A striking feature of the attacks is that the rapid forward lunge of the copepod normally does not create a fluid disturbance that significantly displaces the prey (Fig. 1); the prey remains almost unaffected by the motion of the copepod until the feeding basket opens and the prey is accelerated toward the mouth (Fig. 2). The average displacement of the prey during the attack jump corresponds to only 3–4% of the body length of the copepod and ranges up to 8% in the larger species and 13% in the smaller (Table 1 and Fig. 1). The unsuccessful attacks included the largest prey displacements.

In direct continuation of the strike the copepod flings out the feeding appendages to capture the prey. In *A. tonsa*, the first swimming legs strike back while the second antennae sweep forward, and the mandibles and 2 sets of maxillae with their long setae are open, thus together creating a flow that sucks in the prey (Fig. 2). The feeding appendages then reverse, thus enclosing the prey. *O. davisae* captures the prey by the second maxillae and the maxillipeds that stretch out immediately after the forward lunge (Fig. 1*A*), creating a suction that accelerates the prey to within reach of the feeding appendages. In both species, the prey accelerates in the capture flow to a speed of $\approx$10 mm·s^{-1} in 2–4 ms over a distance of 50–100 μm. In *A. tonsa* >1 fling is often required before the prey is captured, up to 7 and on average 2.5 flings, and the number of flings and the time to capture are directly correlated to the postjump distance to the prey ($P < 0.1\%$ in both cases). *O. davisae* mostly captures the prey in the first fling, although one case required 3 flings (average 1.3 flings). During these attempts the prey is moved at a high velocity that fluctuates with the beating of the appendages (Fig. 2 *B* and *E*), but there is no apparent further adjustment of the position of the copepod in response to the changing position of the prey. Hence, some prey are lost. During the postjump flings, the swimming legs are kept together but move back and

Table 1. Statistics of prey attacks in *A. tonsa* and *O. davisae*

	A. tonsa			*O. davisae*		
Property	Average (range)	SD	*n*	Average (range)	SD	*n*
Size of copepod (Prosome), mm	0.81	0.04	60	0.32	0.01	60
Detection distance (distance of prey to first antenna), mm	0.11 (0–0.21)	0.07	21	0.12 (0.03–0.38)	0.09	22
Jump distance, mm	0.24 (0–0.68)	0.16	20	0.18 (0–0.47)	0.11	21
Distance to mouth after jump, mm	0.18 (0–0.29)	0.05	20	0.09 (0.05–0.14)	0.03	18
Prey displacement during attack jump, mm	0.022 (0–0.064)	0.017	18	0.012 (0–0.041)	0.011	18
Duration jump (detect to open feeding appendages), ms	6.8 (4.2–15.3)	2.8	19	5.1 (2.1–31.3)	6.4	19
Duration (detect-capture), ms	32 (7–107)	28	15	9 (2.6–29.5)	7	18
Capture success	0.75		20	0.86		21

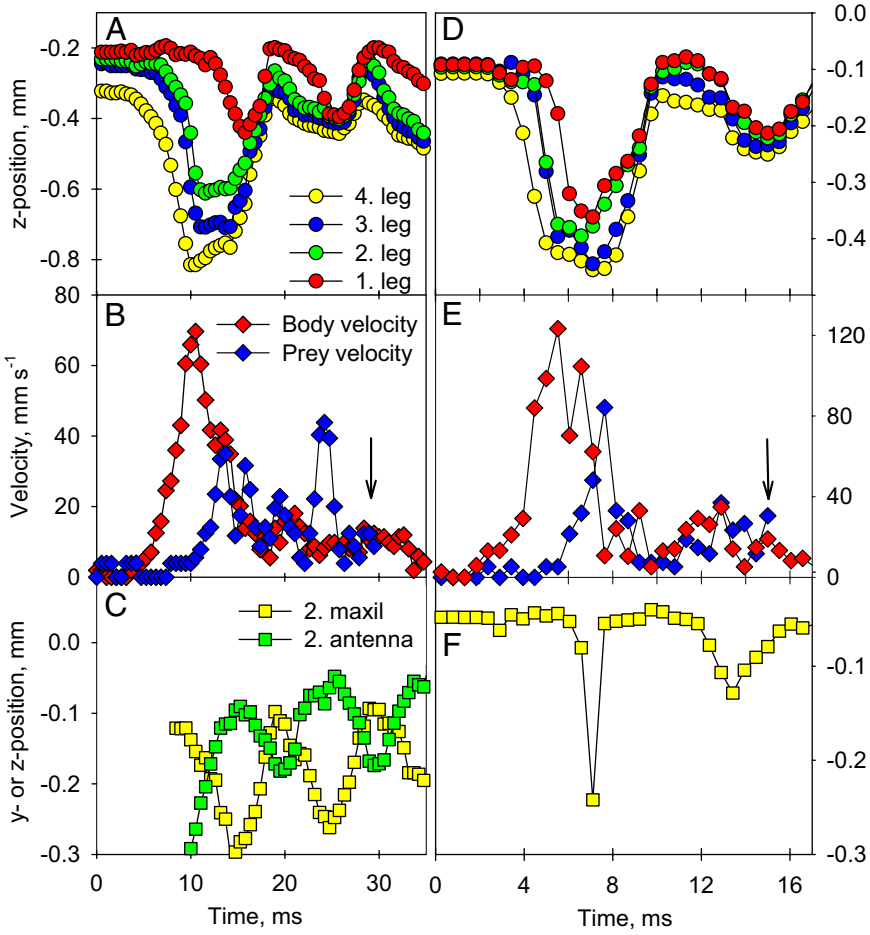

Fig. 2. Kinematics of prey attacks in *A. tonsa* (*A–C*) and *O. davisae* (*D–F*) described by the temporal variation in the position of the tips of various appendages (relative to a coordinate system that has the tip of the head as origin and the *z* axis aligned with the body axis) and in the velocity of the copepod and its prey particle (relative to a fixed coordinate system). Arrows in *B* and *E* indicate final capture of prey. The position of the second maxil in *A. tonsa* (*C*) is given as the *y*-coordinate; *z*-positions are given for all other appendages.

forth, in counter phase with the feeding appendages, thus reducing the forward motion of the copepod that the beating feeding appendages would otherwise cause (Fig. 2 *A* and *D*).

We observed a few escape jumps in both copepod species. These are similar to attack jumps in that the 4 functional swimming legs beat sequentially backwards, the posterior legs first, followed by the joint recovery of the legs. Several such beat cycles and groups of beat cycles may follow one another. During the power stroke, *A. tonsa* accelerates from 0 to up to 4–500 mm·s^{-1} in 4 ms, and *O. davisae* accelerates from 0 to up to 120 mm·s^{-1} in 4 ms. Thus, peak velocities during escapes are much higher than attack speeds in the larger species, whereas the smaller species seem to use their maximum jump speed during attacks.

Discussion

The movement of the feeding appendages and the actual capture of the prey described here is very similar to that described for copepods that generate feeding currents (13), but the prey encounter mechanisms differ. During the attack-jump the prey is typically displaced insignificantly, which is key to a successful attack (Fig. 1 and Table 1). We argue that the flow in the vicinity of the prey can be approximated by potential flow and that the viscous boundary layer surrounding the moving copepod is thin. Viscosity is ignored in potential flow and the disturbance created by a moving body is solely caused by water pushed away to allow room for the translating body; it hence decreases with the inverse cube of the distance to the body. As the copepod accelerates from rest, the thickness of the viscous boundary layer grows diffusively as $\delta \sim (\nu t)^{1/2}$, where ν is the kinematic viscosity and t is time (21). One could therefore expect that the duration of the jump determines the maximum boundary layer thickness, but it turns out that the jump kinematics puts an important constraint on the problem. Assuming constant acceleration in a jump of one body length, L, and duration T, the peak velocity of the copepod is $U_{max} = 2L/T$, which implies that the boundary layer thickness during the attack grows to $\delta \sim (\nu T)^{1/2} = (2L\nu/U_{max})^{1/2}$, which is similar to the thickness that would be found if the body was moving with constant velocity U_{max}. Thus the relative boundary layer thickness at the end of the attack jump is characterized solely by the maximum Reynolds number $\mathrm{Re} = LU_{max}/\nu$ and decreases with increasing Reynolds number as $\delta/L \sim \mathrm{Re}^{-1/2}$. (Because feeding appendages scale with L, it is the relative distances that matter.) Simulated flow fields generated by an idealized attack jump show that the boundary layer thickness is almost constant on the anterior part of the body (Fig. 3*B*) because of the rearward acceleration of the fluid outside the boundary layer from the front stagnation point. The Reynolds numbers for the two examined species varied between 30 and 100. The typical position of the prey at the end of the attack jump is well outside the boundary layer for Reynolds numbers larger than a critical value Re_c somewhere between 10 and 100 (Fig. 3

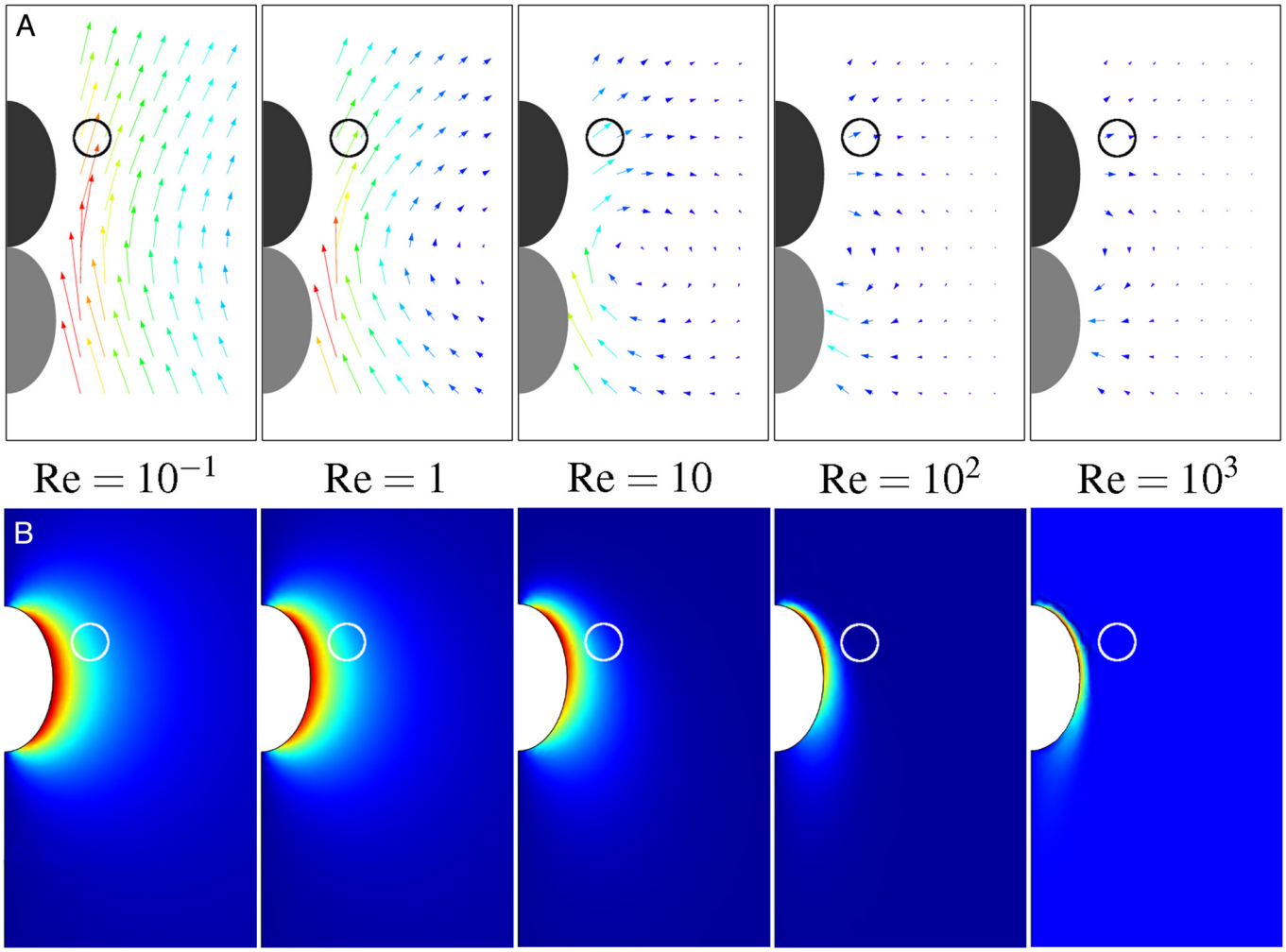

Fig. 3. Displacement of passive prey particles between the beginning and end of an attack jump (*A*) and vorticity (indicative of boundary layer) around the model copepod at end of jump (*B*) for different Reynolds numbers. In the simulations the Navier–Stokes equations are solved in an accelerated reference frame modeling the kinematics of the jump without taking into account the specific swimming leg movements generating the thrust. Typical prey positions at end of jump are indicated by circles. The length of the simulated attack jump is 1 body length; shorter attack jumps yield shorter prey displacements.

A and *B*), and the estimated displacement of prey therefore corresponds to <10% of the body length of the attacking copepod, consistent with observations (Table 1). In the regime $\mathrm{Re} > \mathrm{Re_c}$, potential theory should be applicable, and we have computed the corresponding prey displacements by using pure potential theory, where the copepod is represented as a sphere (see *SI Appendix*). The prey displacement only depends on the initial and final positions of the copepod and not on the details of the motion. The results are indeed similar to the simulations at large Re and we have obtained an analytic expression valid for small displacements. For a copepod making a jump of 1 body length along a fixed axis, a prey particle in the equatorial plane of the sphere, at a distance s from the axis will be displaced approximately $d = 0.5\,L(s/L)^{-2}$, which thus decays rapidly with distance.

The requirement for high acceleration and velocity during the attack jump restricts the strategy to larger forms. This follows from an analysis of power requirements for rapid jumps: The mass-specific power production required to jump with a given Re scales with L^{-4} (see *SI Appendix*). The muscle-mass-specific power production in jumping copepods is much higher than reported for other invertebrate groups and similar to the highest estimated for vertebrates and it is roughly size independent (see *SI Appendix* and refs. 22 and 23); there will therefore be a critical lower size limit for effective attack jumps where $\mathrm{Re_c}$ is reached. The same follows from empirical data: At peak performance, assessed from escape jumps in copepods, acceleration and maximum velocities both scale approximately with $L^{0.6}$ and hence the relative thickness of the boundary layer scales with $\delta/L \sim L^{-0.8}$ and increases dramatically for copepods smaller than ≈1/4 mm (Fig. 4). Thus, the small *O. davisae* is close to this critical size and must use its maximum potential during attacks, in contrast to the larger *A. tonsa* that may escape substantially faster (500 mm·s^{-1}) than it attacks (24).

Many motile microplankton prey, both copepod nauplii and protists, are capable of perceiving and escaping fluid disturbances; they react to fluid deformation rates >1–5 s^{-1} by escaping at velocities of up to 1 cm·s^{-1}, which allows them to escape typical zooplankton feeding currents (17, 25). At the typical position of the prey, deformation rates computed from our simulation exceed 5 s^{-1} at $\mathrm{Re} \geq 10$ at the end of the attack jump and the prey is thus warned. However, the duration of signals exceeding a threshold of 1 s^{-1} is rather short, for example at most 6 ms for the smallest and 13 ms for the larger of our two examined species. During this time the prey may at worst escape a distance of 0.06 and 0.13 mm, respectively, corresponding to

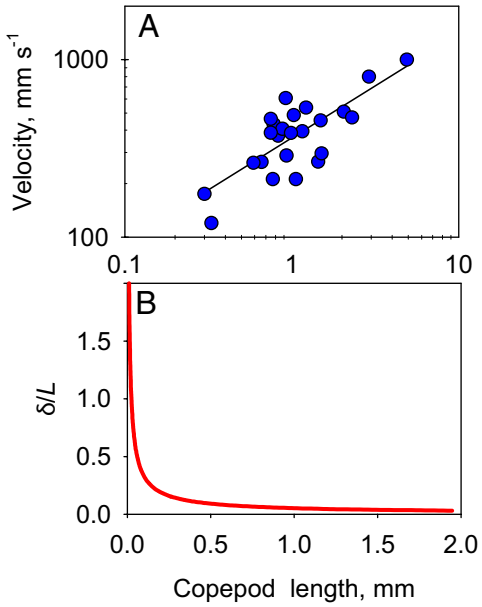

Fig. 4. Escape velocities (U) of copepods (A) regressed against body length (L) [$U = U_0\,(L/L_0)^{0.6}$, with $U_0\,L_0^{-0.6} = 4{\cdot}10^2$ mm$^{0.4}{\cdot}$s^{-1}] is used to estimate the relative boundary layer thickness ($\delta/L \sim \mathrm{Re}^{-1/2}$) as a function of copepod size (B). Escape velocities include those reported here and data from the literature (22, 24, 28, 30–33). The observed velocity exponent reflects the intermediate Reynolds numbers for escaping copepods. At low Reynolds number (linear drag) we would expect a linear dependence on L, and at high Reynolds number (quadratic drag) we would expect that the maximum velocity is independent of L because muscle force scales as L^2.

≤20% of predator body length, provided instantaneous prey reaction [latency times in protists may be 1–10 ms (26)]. Smaller or slower attackers may allow prey sufficient time to escape longer relative distances and hence this aspect also restricts the strategy to larger forms.

A final key to a successful attack is exact 3D information on the position of the prey. Copepods are blind and use the mechanosensory setae distributed on the first antenna to perceive motile prey in the water (15). Such a sensory arrangement permits exact 3D determination of the position and velocity of the prey (16). During the forward lunge, which lasts only a few milliseconds, the copepod is unlikely to receive new information on the position of the prey, because the transmission time of signals through the antenna is 2–10 ms (27, 28), similar to the duration of the attack jump. The copepod also does not seem to readjust to the changing position of the prey during the postjump capture attempts, where any fluid signal from the swimming prey is likely overridden by the complex flow generated by the beating appendages. Thus, the precision of the initial strike is essential.

Common for the two taxonomically distant groups of zooplankton that hold most of the zooplankton ambush feeders with active prey attack is that they both have very well-developed prey perception capabilities with similar spatial arrangements of mechanosensory setae (29). The streamlined arrow- or torpedo-shaped bodies of chaetognaths and copepods and the unusually powerful musculature of at least copepods (22, 13) allow for the fast attack jumps that are essential to high prey capture success. Fish larvae, while not ambushers, also capture prey by rapid surprise attacks and share many of the same features. These necessary features are not found in other planktonic groups. The restrictive requirements to the body plan of a planktonic ambush feeder with surprise attacks may help explain why this strategy, although highly successful, has evolved to perfection only a few times.

Materials and Methods

Experimental Organisms. The copepods were supplied from continuous laboratory cultures. As motile prey in the experiments we used the dinoflagellate *Oxhyrris marina* for *O. davisae*, and ciliates, *Strombidium sulcatum*, for *A. tonsa*. *O. marina* measures 18 (SD ± 3) μm in diameter and swims at ≈0.37 (SD ± 0.09) mm·s^{-1} and *S. sulcatum* measures 27 (SD ± 2) μm in diameter and swims at ≈0.59 (SD ± 0.15) mm·s^{-1}.

Observations and Experiments. Recordings were made with a Phantom v4.2 Monochrome high-speed digital video camera operated at frame rates of 1,600–2,200 frames per s, a resolution of 512 × 512 pixels, and of storage capacity of 2,000 frames. Observations of attacks were made in 69 mL aquaria with copepods and protists added. The camera lenses yielded a field of view of ≈3 × 3 or 1.4 × 1.4 mm^2. Observations of escape jumps were made in 1 L aquaria at lower magnification. Illumination to provide shadow images was provided by a 50-W halogen bulb. All experiments were conducted at room temperature. We recorded 22 attacks and 3–6 escapes in each species. All attacks were recorded from various angles, and none of the records allowed us to see all details.

Kinematic Description of Prey Attacks. The attacks that revealed most details (6 for *A. tonsa* and 3 for *O. davisae*) were analyzed thoroughly, whereas only selected parameters were extracted from the remaining attacks. Using shareware ImageJ (manual tracking) we digitized frame-by-frame the position of the copepod (tip of head, end of body) and the position of the tips of the urosome, each of the feeding appendages (that could be seen), the 4 anterior swimming legs (the fifth swimming leg is rudimentary in *A. tonsa*, and *O. davisae* has only 4 pairs of swimming legs), and the position of the prey. The position of the urosome and appendages were subsequently transformed into a coordinate system that had the tip of the head as origin and the z-axis aligned with the length direction of the body. Velocities were computed on basis of the trajectories. All distances are 2D projections of 3D distances and therefore underestimated.

Simulations. We modeled the body of the copepod as an ellipsoid of major axis L and minor axis $W = 2/3L$. It was moved along the z-axis over a distance equal to its body length L, and the duration of the jump was T (Fig. S1). Its motion was prescribed with the assumption of a constant acceleration, $a = 2L/T^2$. Velocity and vorticity fields were computed by solving the Navier-Stokes equations using the commercial software Comsol. The equations were solved in the accelerated reference frame of the copepod and in cylindrical polar coordinates (s, z, φ). The time step was $dt = T/200$. A no-slip boundary condition was applied at the ellipsoid surface. The ellipsoid was placed at the center of a cylindrical domain of height $30L$ and radius $15L$. On the external walls of the domain, the s- and z-components of the velocity had to satisfy $u_s = 0$ and $u_z = -U(t)$. The prey was assumed neutrally buoyant and passive, and therefore to follow the particle paths. Trajectories of tracers initially placed on a regular grid were computed by integrating the velocity field at each time step. We computed the deformation field from the strain-rate matrix, which was interpolated at each time step and then diagonalized. From the 3 eigenvalues λ_i, i = 1, 2, 3, we defined the scalar deformation rate as: $\varepsilon_{max} = \max(|\lambda_1|,|\lambda_2|,|\lambda_3|)$.

ACKNOWLEDGMENTS. This work was supported by a grant from the Danish Council for Independent Research, Natural Sciences.

1. Hansen PJ, Bjørnsen PK, Hansen BW (1997) Zooplankton grazing and growth: Scaling within the 2- to 2,000-μm body size range. *Limnol Oceanogr* 42:687–704.
2. Fenchel T (1986) The ecology of heterotrophic microflagellates. *Adv Microb Ecol* 9:57–97.
3. Flood PR (1991) Architecture of, and water circulation and flow rate in, the house of the planktonic tunicate *Oikopleura labradoriensis*. *Mar Biol* 111:95–111.
4. Dalpadado P, Yamaguchi A, Ellertsen B, Johannessen S (2008) Trophic interactions of macro-zooplankton (krill and amphipods) in the Marginal Ice Zone of the Barents Sea. *Deep Sea Res II* 55:2266–2274.
5. Jonsson PR, Tiselius P (1990) Feeding behavior, prey detection, and capture efficiency of the copepod *Acartia tonsa* feeding on planktonic ciliates. *Mar Ecol Prog Ser* 60:35–44.
6. Feigenbaum D, Reeve MR (1977) Prey detection in Chaetognatha: Response to a vibrating probe and experimental determination of attack distance in large aquaria. *Limnol Oceanogr* 22:1052–1058.
7. Svensen C, Kiørboe T (2000) Remote prey detection in *Oithona similis*: Hydromechanical vs. chemical cues. *J Plankton Res* 22:1155–1166.
8. Costello JH, Colin SP, Dabiri JO (2008) Medusan morphospace: Phylogenetic constraints, biomechanical solutions, and ecological consequences. *Inv Biol* 127:265–290.

9. Galienne CP, Robins DB (2001) Is *Oithona* the most important copepod in the world's oceans? *J Plankton Res* 23:1421–1432.
10. Paffenhöfer GA (2006) Oxygen consumption in relation to motion of marine planktonic copepods. *Mar Ecol Prog Ser* 317:187–192.
11. Castellani C, Robinson C, Smith T, Lampitt RS (2005) Temperature affects respiration rate of *Oithona similes. Mar Ecol Prog Ser* 285:129–135.
12. Eiane K, Ohman MD (2004) Stage-specific mortality of *Calanus finmarchicus*, *Pseudocalanus elongatus*, and *Oithona similis* on Fladen Ground, North Sea, during a spring bloom. *Mar Ecol Prog Ser* 268:183–193.
13. Koehl MAR, Strickler JR (1981) Copepod feeding currents. Food capture at low Reynolds number. *Limnol Oceanogr* 26:1062–1073.
14. Andrews DJ (1983) Deformation of the active spaces in the low Reynolds number feeding current of calanoid copepods. *Can J Fish Aquat Sci* 40:1293–1302.
15. Strickler JR (1975) Intra- and interspecific information flow among planktonic copepods receptors. *Verh Internat Verein Limnol* 19:2951–2958.
16. Jiang H, Paffenhöfer GA (2008) Hydrodynamic signal perception by the copepod *Oithona plumifera*. *Mar Ecol Prog Ser* 373:37–52.
17. Jakobsen HH (2002) Escape of protists in predator-generated feeding currents. *Aquat Microb Ecol* 26:271–281.
18. Nakamura Y, Turner JT (1997) Predation and respiration by the small cyclopoid copepod *Oithona similis*: How important is feeding on ciliates and heterotrophic flagellates? *J Plankton Res* 19:1275–1288.
19. Saiz E, Calbet A, Broglio E (2003) Effects of small-scale turbulence on copepods: The case of *Oithona davisae. Limnol Oceanogr* 48:1304–1311.
20. Kiørboe T, Visser AW (1999) Predator and prey perception in copepods due to hydromechanical signals. *Mar Ecol Prog Ser* 179:81–95.
21. Batchelor GK (1967) *An Introduction to Fluid Dynamics* (Cambridge Univ Press, Cambridge, UK).
22. Lenz PH, Hower AE, Hartline DK (2004) Force production during pereiopod power strokes in *Calanus finmarchicus*. *J Mar Systems* 49:133–144.
23. Askew GN, Marsh RL (2002) Review: Muscle designed for maximum short-term power output: Quail flight muscle. *J Exp Biol* 205:2153–2160.
24. Buskey EJ, Lenz PH, Hartline DK (2002) Escape behavior of planktonic copepods in response to hydrodynamic disturbances: High-speed video analysis. *Mar Ecol Prog Ser* 235:135–146.
25. Titelman J, Kiørboe T (2003) Predator avoidance by nauplii. *Mar Ecol Prog Ser* 247:137–149.
26. Machemer H, Deitmer JW (1985) in *Progress in Sensory Physiology*, ed Ottoson D (Springer, Berlin), pp 81–118.
27. Lenz PH, Hartline DK, Davis AD (2000) The need for speed. I. Fast reactions and myelinated axons in copepods. *J Comp Phys A* 186:337–345.
28. Waggett RJN, Buskey EJ (2008) Escape reaction performance of myelinated and nonmyelinated calanoid copepods. *J Exp Mar Biol Ecol* 361:111–118.
29. Feigenbaum DL (1978) Hair fan patterns in the Chaetognatha. *J Can Zool* 56:536–546.
30. Yen J, Strickler JR (1996) Advertisement and concealment in the plankton: What makes a copepod hydrodynamically conspicuous? *Inv Biol* 115:191–205.
31. Waggett RJ, Buskey EJ (2007) Calanoid copepod escape behavior in response to a visual predator. *Mar Biol* 150:599–607.
32. Koga F (1984) The developmental stages of *Temora turbinate* (Copepoda: Calanoida). *Bull Plankton Soc Japan* 31:43–52.
33. Burdick DS, Hartline DK, Lenz PH (2007) Escape strategies in co-occurring calanoid copepods. *Limnol Oceanogr* 52:2373–2385.

Supporting Information

Kiørboe et al. 10.1073/pnas.0903350106

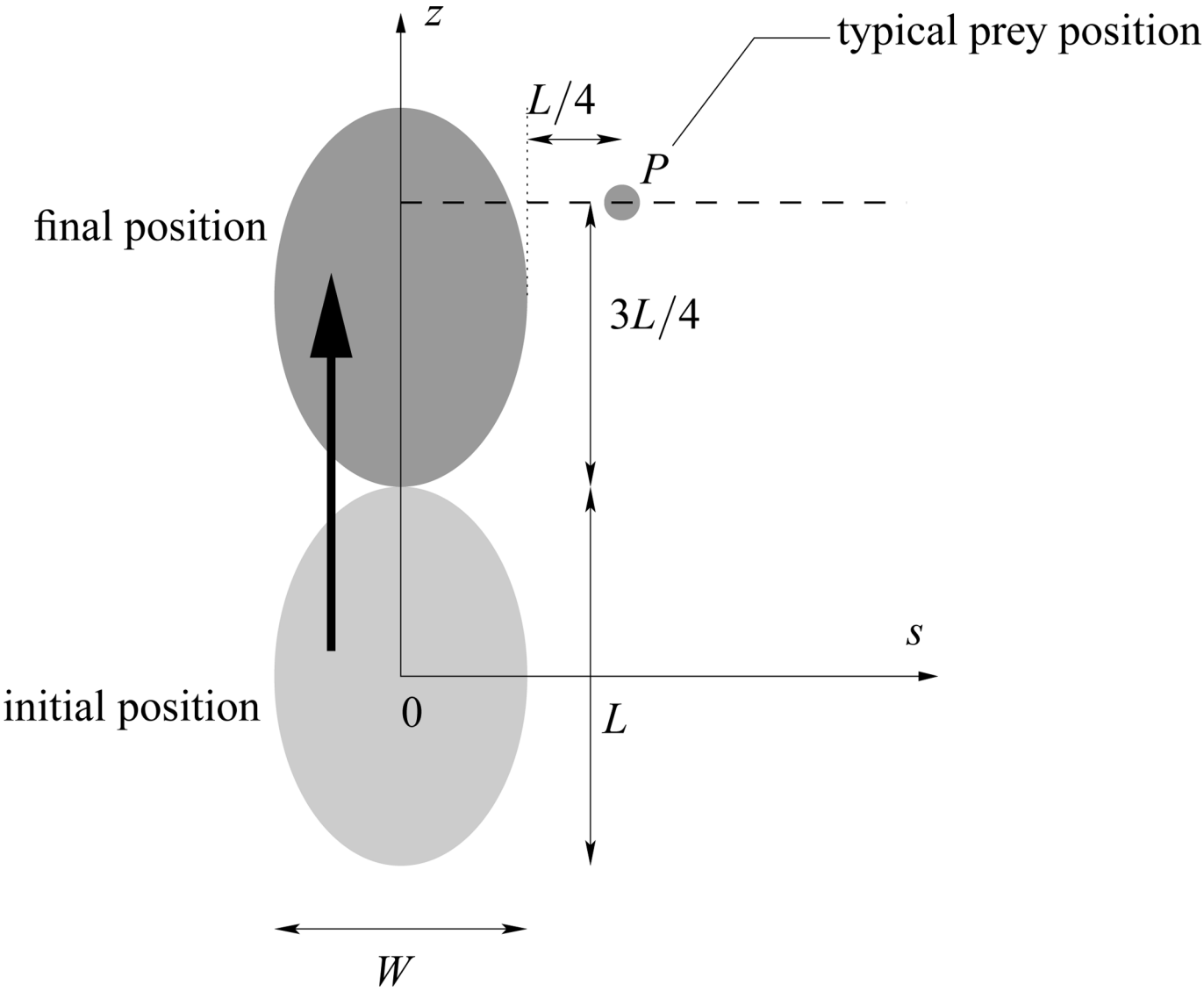

Fig. S1. The model copepod performing a jump of 1 body length, *L*. The initial (light gray ellipsoid) and final (dark gray ellipsoid) position of the copepod, and the typical position of the prey at the end of the jump are indicated.

Movie S1. Examples of *A. tonsa* attacking motile ciliates, *Strombidium sulcatum*, played in slow motion at 1/270× real time. During the forward jump, the prey remains almost stationary (the swimming of the prey is negligible at this time scale). In many cases the copepod does not manage to capture the prey in the first attempt with the feeding appendages, and the prey is moved around by the beating feeding appendages until eventually captured (or lost). The imposed velocity of the prey during this period by far exceeds its escape jump capacity.

Movie S1 (MOV)

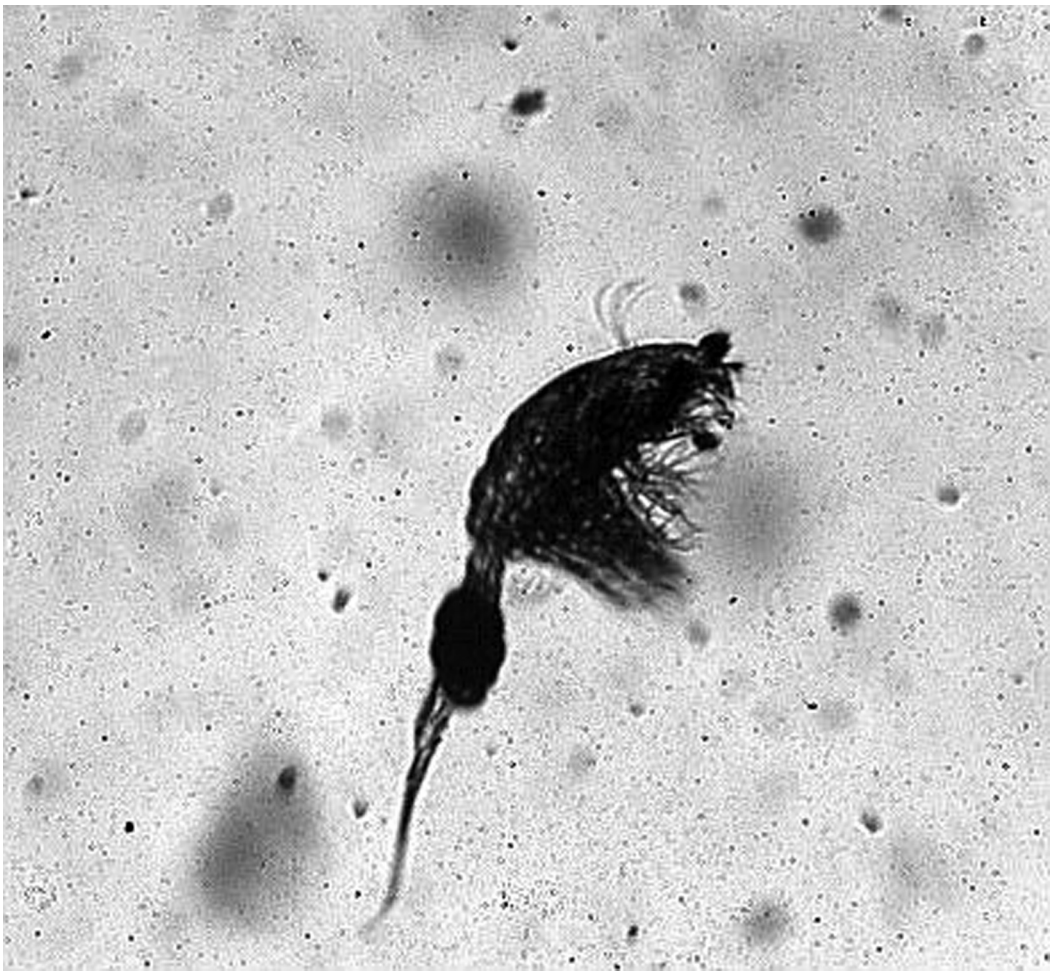

Movie S2. Examples of *O. davisae* attacking motile dinoflagellates, *Oxhyrris marina*, played in slow motion at 1/270× real time. In this species, the prey is almost always captured in the first attempt. Note again that the prey does not move significantly during the forward lunge of the copepod.

Movie S2 (MOV)

Other Supporting Information Files

SI Appendix (PDF)

Supporting Information

POTENTIAL FLOW

We here show that potential theory provides a good description of the flow field around the copepod at the typical position of the prey, as its predictions compare well to both the results of the full simulations (Fig. 3) and the observations (Table 1).

For simplicity we shall represent the copepod as a sphere with radius R chosen as the half minor axis of the ellipsoid, i.e., $R = W/2$, so the major axis of the ellipsoid is $L = 3R$. The center of the sphere $\mathbf{r}_c$ moves with velocity $\mathbf{U(t)} = \mathbf{r}_c'(t)$. For motion along the positive z-axis, the velocity field is given as the gradient of the velocity potential (1)

$$\phi(r,\theta,t) = -\frac{U(t)R^3}{2r^2}\cos\theta \qquad \text{(S1)}$$

where r and θ are spherical coordinates around the instantaneous center of the sphere $\mathbf{r}_c$. Note that the velocity potential (and therefore the entire velocity field) is proportional to the instantaneous velocity and *independent* of the acceleration. Potential theory is valid as long as the flow has no vorticity and this is true at short time scales and high Reynolds numbers since we assume that the sphere moves into quiescent fluid and the boundary layers do not reach into the region of flow considered. It should be noted that the description in terms of potential theory would not work well for the flow *behind* the copepod, since here the flow would be progressively disturbed by separating boundary layers and the effects of the swimming legs would be significant.

A small, neutrally buoyant prey particle in the fluid satisfies the equation of motion

$$\frac{d\mathbf{r}}{dt} = U(t)\mathbf{v}^{(\mathbf{0})}(\mathbf{r} - \mathbf{r}_c(t)) \qquad \text{(S2)}$$

where $\mathbf{v}^{(0)}$ is the velocity field for a sphere at the origin moving with unit velocity along the *z*-axis. In cylindrical coordinates (s,z) we can write

$$\begin{aligned}\frac{ds}{dt} &= U(t)v_s^{(0)}(s,z-z_c(t))\\ \frac{dz}{dt} &= U(t)v_z^{(0)}(s,z-z_c(t))\end{aligned} \tag{S3}$$

and we are interested in determining the displacement of a particle from its original position (s_0,z_0) to its final position $(s(t_f),\ z(t_f))$, i.e., $d=\sqrt{(s(t_f)-s_0)^2+(z(t_f)-z_0)^2}$. Using $x = z - z_c(t)$ as independent variable instead of time this can be written

$$\begin{aligned}\frac{ds}{dx} &= -v_s^{(0)}(s,x) = -\frac{3R^3}{2}\frac{xs}{\left(s^2+x^2\right)^{5/2}}\\ \frac{dz}{dx} &= -v_z^{(0)}(s,x) = -\frac{R^3}{2}\frac{2x^2-s^2}{\left(s^2+x^2\right)^{5/2}}\end{aligned} \tag{S4}$$

where now $U(t) = z_c'(t)$ has dropped out and the displacements thus only depend on the length that the sphere moves, not on the details of the time history. This is typical of potential flow.

In analogy to the ellipsoidial model, the prey is assumed to be in the equatorial plane of the sphere in the final position, i.e., $z_0 = L = 3R$ and at a distance *L*/4 from the surface, i.e., $s_0 = 1.75\ R$. For this configuration we get the displacements

$$\Delta s \approx 0.1267R,\ \Delta z \approx -0.0279R \text{ and } d=\left((\Delta s)^2+(\Delta z)^2\right)^{1/2} \approx 0.1297R = 0.0432L \tag{S5}$$

The simulation for the ellipsoid above gives $d \approx 0.0525L$ at Re=1000, and the correspondence is quite good considering the spherical approximation.

To get an approximate analytical expression for the displacements we exploit the rapid decay of the velocity field away from the center of the sphere, which means that we get a reasonable

approximation by neglecting the small variations of s and z on the right hand side of Equation (S4). This makes the system integrable and we find

$$\begin{aligned}\Delta s &= s(x_f) - s_0 = \frac{R^3 s_0}{2\left(s_0^2 + (z_0 - x_f)^2\right)^{3/2}} - \frac{R^3 s_0}{2\left(s_0^2 + z_0^2\right)^{3/2}} \\ \Delta z &= z(x_f) - z_0 = \frac{R^3 (z_0 - x_f)}{2\left(s_0^2 + (z_0 - x_f)^2\right)^{3/2}} - \frac{R^3 z_0}{2\left(s_0^2 + z_0^2\right)^{3/2}}\end{aligned} \tag{S6}$$

For $x_f = z_0$, i.e., the situation where the prey is in the equatorial plane in the final position we get

$$\begin{aligned}\Delta s &= \frac{R^3}{2s_0^2} - \frac{R^3 s_0}{2\left(s_0^2 + z_0^2\right)^{3/2}} \\ \Delta z &= -\frac{R^3 z_0}{2\left(s_0^2 + z_0^2\right)^{3/2}}\end{aligned} \tag{S7}$$

which means that the displacement $d = \sqrt{\Delta s^2 + \Delta z^2}$ can be expressed in terms of s_0 and $r_0 = \sqrt{s_0^2 + z_0^2}$ as

$$d = \frac{R^3}{2s_0^2}\left(1 - 2\left(\frac{s_0}{r_0}\right)^3 + \left(\frac{s_0}{r_0}\right)^4\right)^{1/2} = \left(\frac{L}{3}\right)^3 \frac{1}{2s_0^2}\left(1 - 2\left(\frac{s_0}{r_0}\right)^3 + \left(\frac{s_0}{r_0}\right)^4\right)^{1/2} \tag{S8}$$

For our standard configuration ($s_0 = 1.75R$ and $z_0 = 3R$) this gives $\Delta s \approx 0.1424R$, $\Delta z \approx -0.0358R$ and $d \approx 0.146831R = 0.04894L$, not far from the results in Equation (S5).

The strain-rates are readily computed in potential theory. Due to rotational symmetry the strain rate tensor is given by

$$\varepsilon = \begin{pmatrix} \varepsilon_{ss} & 0 & \varepsilon_{sz} \\ 0 & \varepsilon_{\varphi\varphi} & 0 \\ \varepsilon_{sz} & 0 & \varepsilon_{zz} \end{pmatrix} = \begin{pmatrix} \dfrac{\partial v_s}{\partial s} & 0 & \dfrac{1}{2}\left(\dfrac{\partial v_z}{\partial s} + \dfrac{\partial v_s}{\partial z}\right) \\ 0 & \dfrac{v_s}{s} & 0 \\ \dfrac{1}{2}\left(\dfrac{\partial v_z}{\partial s} + \dfrac{\partial v_s}{\partial z}\right) & 0 & \dfrac{\partial v_z}{\partial z} \end{pmatrix} \tag{S9}$$

For a prey-particle at position (*s,z*) with distance $r = \sqrt{s^2 + z^2}$ (all measured from the position of the sphere moving at velocity U) the instantaneous eigenvalues for the strain rate tensor are

$$\varepsilon_{1,2} = \frac{3UR^3}{4r^4}\left(-\frac{z}{r} \pm \sqrt{4 + 5\left(\frac{z}{r}\right)^2}\right)$$
$$\varepsilon_3 = UR^3\frac{3z}{2r^5} \qquad \text{(S10)}$$

The magnitude of the strain rate in the equatorial plane of the sphere ($z = 0$), where $\varepsilon_1=\varepsilon_2$ and $\varepsilon_3=0$, is

$$\varepsilon = \frac{3UR^3}{2s^4} \qquad \text{(S11)}$$

The maximal velocity entering this expression is, assuming constant acceleration,

$$U = U_{\max} \approx \frac{2L}{T} = \frac{6R}{T} \qquad \text{(S12)}$$

where T is the duration of the attack, and the maximum strain rate at $s = 1.75\ R$ is

$$\varepsilon_{max} \approx \frac{9}{1.75^4 T} \approx \frac{0.96}{T} \qquad \text{(S13)}$$

For at typical value $T = 10$ ms we get $\varepsilon_{max} \approx 100\ \mathrm{s}^{-1}$.

POWER REQUIREMENTS FOR RAPID JUMPS

A rough estimate of the average power required for rapid jumps can be achieved as follows. During the jump, the force which the copepod must produce to accelerate and overcome drag is

$$F = (3/2)\ m\ (\mathrm{d}U/\mathrm{d}t) + D, \qquad \text{(S14)}$$

where the first term takes the added mass effect into account (m is the copepod mass and U is the copepod velocity), and the 2nd term is the drag force. We model the copepod as a sphere and take $D = (1/2)\ \pi\ \rho\ R^2\ C_D\ U^2$, where R is the radius of the copepod, ρ is its density, and

$C_D = 24/\mathrm{Re}+5/\mathrm{Re}^{1/2}+2/5$ (2). We assume constant acceleration of an attack jump of 1 body length, $L = 2R$, of duration T and to a maximum velocity U_{max}. The average power integrated over the power stroke of the jump is then

$$P = \frac{1}{T}\int_0^T F(t)U(t)dt = \frac{3mU_{\max}^2}{4T} + \pi\rho R^2 U_{\max}^3\left(\frac{4}{\mathrm{Re}} + \frac{5}{7\sqrt{\mathrm{Re}}} + \frac{1}{20}\right). \quad \text{(S15)}$$

Recalling that $U_{max} = 2L/T$ the mass specific average power $P^* = P/m$ is then

$$P^* = \frac{3U_{\max}^3}{4R}\left(\frac{4}{\mathrm{Re}} + \frac{5}{7\sqrt{\mathrm{Re}}} + \frac{3}{10}\right). \quad \text{(S16)}$$

To achieve a given Reynolds number ($\mathrm{Re} = 2\,R\,U_{\max}/v$) in the jump, it follows that the mass specific power scales with size as

$$P^* \propto L^{-4} \quad \text{(S17)}$$

where $L = 2R$. Thus, power requirements for attack jumps increase dramatically with declining size of the predator.

References

1. Batchelor G K (1967) *An Introduction to Fluid Dynamics*. Cambridge University Press, Cambridge.
2. Lautrup B (2005) *Physics of Continuous Matter*. Institute of Physics Publishing, Bristol.